Accepted Manuscript

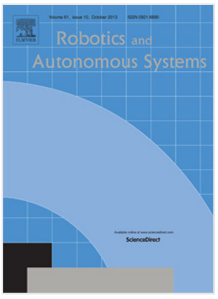

Feasible acceleration count: A novel dynamic stability metric and its use in incremental motion planning on uneven terrain

Arun Kumar Singh, K.Madhava Krishna

PII: S0921-8890(15)00295-X
DOI: http://dx.doi.org/10.1016/j.robot.2015.11.007
Reference: ROBOT 2577

To appear in: *Robotics and Autonomous Systems*

Received date: 20 May 2014
Revised date: 10 November 2015
Accepted date: 16 November 2015

Please cite this article as: A.K. Singh, K.M. Krishna, Feasible acceleration count: A novel dynamic stability metric and its use in incremental motion planning on uneven terrain, *Robotics and Autonomous Systems* (2015), http://dx.doi.org/10.1016/j.robot.2015.11.007

Feasible Acceleration Count: A Novel Dynamic Stability Metric and its use in Incremental Motion Planning on Uneven Terrain

Arun Kumar Singh and K.Madhava Krishna

Robotics Research Center, IIIT-Hyderabad
*

Abstract

Application of wheeled mobile robots have gradually progressed from the confines of structured indoor environments to rough outdoor terrains. Material transport and exploration are some of the few areas where wheeled robots are required to navigate over uneven terrains. Stable and efficient navigation of wheeled robots over uneven terrains require a framework which can correctly ascertain the stability and maneuverability for a given robot's state. Most existing works on uneven terrain navigation assumes a one-to-one correspondence between postural stability and maneuverability. In this paper, we show that such characterization is incomplete as states having high postural stability may have restricted maneuverability depending on underlying terrain topology. We thus, present a novel metric called *Feasible Acceleration Count* (FAC), introduced in our earlier works as an unified measure of robot stability and maneuverability. The metric gives the measure of the space of feasible accelerations available to the robot at a given state. The feasibility is decided by a set of inequalities which depends not only on robot's state but also on surface normals at the wheel ground contact point. This unique feature of the FAC metric makes it a more appropriate choice for motion planning on uneven terrains than metrics like Tip-Over. We further show that since space of feasible accelerations

*Corresponding author
Email address: arunkumar.singh@research.iiit.ac.in ()

is a direct characterization of the space of possible motions at a given state, the metric *FAC*, also quantifies the quality of state space exploration achieved at each step of incremental sampling based planners. We build on top of this aspect of *FAC* and present an incremental trajectory planner with a novel node selection criteria for navigation of generic four wheeled robots and articulated systems like mobile manipulators on uneven terrain.

Keywords: Uneven Terrain, Feasible Acceleration Count, Incremental Motion Planning, RRT

1. Introduction

With the advent of outdoor robotics and as more and more robots operate outdoors they are entailed to navigate over terrains that are uneven. These require some paradigm changes in robot motion planning methodologies. In particular, one is required to go beyond usual geometric and kinematic motion planning towards algorithms that integrate notion of stability and maneuverability into trajectory planning algorithm. Most existing literature on uneven terrain navigation assume a direct correlation between postural stability and maneuverability. However, such characterization is incomplete as states with high postural stability may have restricted maneuverability depending on the topology of the underlying terrain. In this paper, an exact mathematical correlation between stability and maneuverability of a robot's state on uneven terrain is presented through a metric called, *Feasible Acceleration Count* (*FAC*). As the name suggests, the proposed metric gives a measure of the space of feasible accelerations available to the robot at a given state. The feasibility is decided by a set of inequalities which depends not only on the robot states, the forces and moments acting on it but also explicitly on the topology of the underlying terrain. It is straightforward to note that the space of accelerations at a given state also characterizes the space of possible motions at that state. Thus, the concept of *FAC* proposed in this paper is central to the adaptation of sampling based planners like Rapidly Exploring Random Trees (RRT) [1] [2], [3]

for motion planning on uneven terrain. To understand this further, note that sampling based planners like RRT relies on integrating the evolution model of the system for discrete set of control inputs. This integration procedure results in an incremental construction of a tree like data structure for the exploration of the state space. Thus, the number of discrete control inputs available for integration directly determines the quality of exploration of the state space. In RRT like frameworks, number of discrete control inputs would depend only on the resolution of discretization. However, as we show later, motion planning on uneven terrain is associated with generic state and control dependent differential constraints. Thus, the space of control inputs available for expansion of tree would depend on the state of the robot and the terrain parameters. If acceleration are taken as control inputs, then FAC gives an exact measure of space of available control inputs and consequently the quality of state space exploration. We build on top of this aspect of FAC and present an incremental trajectory planner with a novel node selection criteria for navigation of generic four wheeled robots and articulated systems like mobile manipulators on uneven terrains.

1.1. Related Work

Stability of wheeled mobile robots on uneven terrains has been addressed in many existing literatures, either in isolation or in the context of motion planning on uneven terrain. One of the most popular metrics for defining the stability of wheeled mobile robots on uneven terrain has been the *force angle measure* or *tip-over* margin, proposed in [4] [5]. It has been used for motion planning on uneven terrains in works like [6], [7], [8], [9], where the objective was to obtain paths, along which at each point the robot posture satisfies the *tip-over* stability constraints. An implicit assumption in these cited works is that high stability of the robot as given by *tip-over* margin also corresponds to high maneuverability. Hence, as such these works do not involve any analysis to ascertain whether how well the robot can maneuver along the computed paths. However, this one to one correspondence between *tip-over* stability and maneuverability is

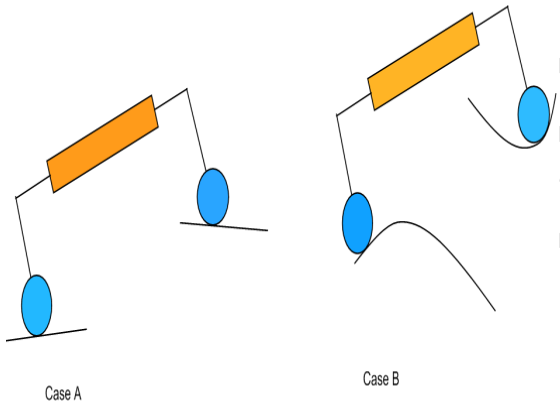

Figure 1: Figure showing front view of two robots which have similar states, forces and moments but are operating on different terrain conditions. Tip-over stability concept would not differentiate between the two cases. However it is quite apparent that the terrain in case A is more favourable for motion than terrain B.

not justified. For example, consider figure 1 which shows two example scenarios where the robots have identical state, forces, moments and wheel ground contact location. The tip-over margin concept would not differentiate between the two cases shown in figure 1. But it is apparent that the topology of the underlying terrain shown in case A is more favorable for motion generation than that shown in case B. In particular the surface normals at wheel ground contact point play an important role in robot maneuverability, but is completely neglected by *tip over* margin concept.

An alternative approach is presented in works like [10], [11], [12], where robot's stability is modelled through a set of constraints which enforce the requirement of permanent contact and no-slip at all the wheel ground contact points. In contrast to *tip-over* margin which primarily captures the postural stability, these set of constraints model stability from the point of view of robot's ability to maneuver and hence is more appropriate for motion planning on uneven terrain. We further strengthen this observation later in the pa-

per. The current proposed work also follows the approach of modeling stability through permanent contact and no-slip constraints. However, we propose some significant and critical advancements in the current state of the art which are necessary for obtaining stable and highly agile trajectories on uneven terrain.

1.2. Contributions

The contributions of the proposed work are synthesized from our earlier results [19], [20] and [21]. However, in contrast to these cited works, the current paper presents a more in-depth analysis of various factors associated with motion planning on uneven terrain. The important aspects of the proposed work can be summarized as follows: Firstly, it provides a more rigorous mathematical representation of permanent contact and no-slip constraints by deriving them from the full 3D dynamics of the robot. This is in contrast to planar model of [10] and point mass model of [11]. The presented 3D constraint model is also an improvement over the procedure presented in [12] where the dynamics are projected into pitch, yaw and roll plane separately. Such procedure requires three different stability computations for each state of the robot. In contrast, the presented framework considers the full 3D dynamic model at once. Moreover, the number of variables in stability computation is same as that in each planar analysis of [12]. Secondly, we incorporate a framework for ascertaining the 6D evolution of the robot's state for a given control input on uneven terrain. Such framework not only forms the crux of obtaining the full 3D dynamics of the robot and consequently the stability constraints, but is also imperative for constructing sampling based motion planners on uneven terrain. Works like [10], [11], [12] do not talk about any such evolution model. Thirdly, we map the solution space of the permanent contact and no-slip constraints to a unified metric called *Feasible Acceleration Count* (FAC) which provides a combined measure of stability, maneuverability and quality of state space exploration achieved at each step of incremental sampling based planners on uneven terrain. This explicit correlation that we describe between FAC and the efficiency of incremental sampling based planners on uneven terrain motion planning problems is a unique

feature of the current proposed work and was not highlighted in [19], [20] and [21]. Fourthly, we develop an incremental trajectory planner with RRT like data structure for motion planning on uneven terrain. However, in contrast to the conventional RRT framework, the proposed incremental planner has a new and novel *FAC* based node selection criteria which has been specifically carved for motion planning on uneven terrain. The proposed planner is applied to generic four wheeled non-holonomic robots as well as to articulated systems like mobile manipulator.

1.3. Layout of the Paper

The rest of the paper is organised as follows. Section 2 presents the framework for computing the 6 *dof* evolution of a generic four wheeled robot on uneven terrain. Section 3 utilises the evolution framework to derive the 3D dynamics of the robot and consequently the permanent contact and no-slip stability constraints. Section 4 describes the procedure for computing the solutions space of stability constraints. It also elucidates the physical significance of the solution space in terms of robot's stability and maneuverability. Section 5 presents the proposed incremental planner and corresponding simulation results are presented in Section 6

2. Robot's 6D Pose Evolution on Uneven Terrains

In this section, we derive the evolution of the robot's 6D pose on uneven terrain purely as a function of robot's geometric parameters and terrain topology. Thus, the derivation presented in this section is applicable to various generic four wheeled passive suspension robots with varied kinematics like skid steered, all wheel steered, Ackerman steered etc., which are extensively used for outdoor explorations, agriculture etc. [13], [14], [15]. To proceed with the derivation, consider a generic four wheeled robot shown in figures 2(a) and 2(b). Let the configuration of the robot at any time t be represented by the $\mathbf{X} = (x, y, \alpha, z, \beta, \gamma)^T$(the notational dependency on variable t is dropped in the

paper for simplicity). For a passive suspension robot, the evolution of robot's yaw plane configuration i.e position (x, y) and heading angle (α) can be directly controlled. The evolution of the rest of the configuration variables i.e z coordinate, roll β and pitch γ are a function of yaw plane configuration and the terrain geometry. Mathematically, this dependency can be represented in the following manner.

$$\begin{cases} z = f_1(x, y, \alpha) \\ \beta = f_2(x, y, \alpha) \\ \gamma = f_3(x, y, \alpha) \end{cases} \tag{1}$$

Obtaining the evolution of 6D pose on uneven terrains reduces to that of obtaining the algebraic form of functions $f_1(.), f_2(.)$ and $f_3(.)$.

It is straightforward to guess that these functions would depend on the terrain geometry. Works like [16], [17] and [18] computes the evolution of a 3 wheeled robot by solving a large set of coupled *differential algebraic equations* (DAE) at each instant of robot's motion. However, these methodologies are computationally intensive and hence it is difficult to incorporate them within a motion planning framework. Moreover, extension of these methodologies to 4 wheeled robot has not been presented in the literature. In our earlier work [19], we proposed a set of coupled non-linear equations which were solved numerically to obtain the complete 6D configuration of the robot. We now present a framework for computing good approximate analytical functional forms for $f_1(.), f_2(.)$ and $f_3(.)$, based on our work [20], [21].

For mapping the yaw plane configuration to the full 6D configuration, we assume that the terrain equation can be known in the following form

$$a = g(b, c) \tag{2}$$

Where a represents the terrain height at the coordinate (b, c). Some works related to generating terrain equations from Digital Elevation Models can be found in [22], [23] and [24]. With the help of terrain equation this section derives analytical functions relating robot's x, y, α to its z coordinate, roll β

and pitch γ. Along with it, x, y, α are also related to the twelve wheel ground contact point variables x_{ci}, y_{ci}, z_{ci}. These relations comes from the holonomic constraints defining the geometry of the robot(refer fig.2(a))

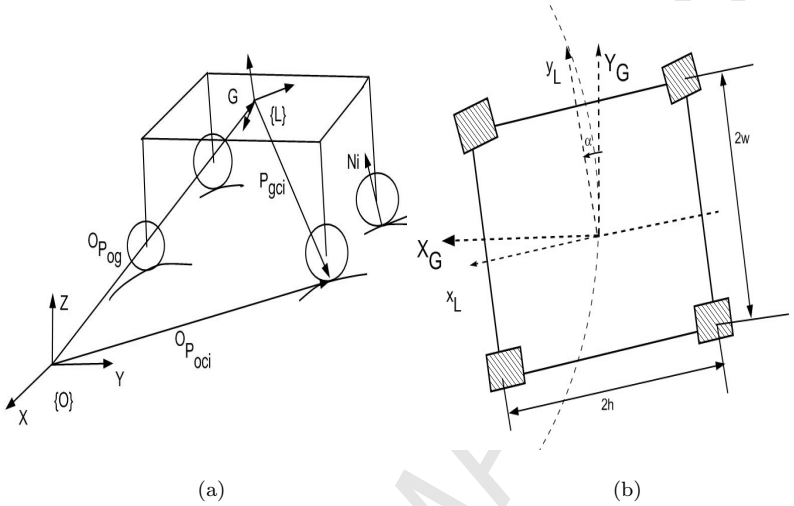

(a) (b)

Figure 2: (a): A four wheeled robot with the vectors describing the holonomic constraint defining the geometry of the robot shown. (b): Top-View of the robot.

$$\overrightarrow{P}_{og} + \overrightarrow{P}_{gci} = \overrightarrow{P}_{oci} \tag{3}$$

where $\overrightarrow{P}_{gci} = \overrightarrow{r}_f$

$\overrightarrow{r}_f = R \begin{bmatrix} \delta_i h & \frac{2.5-i}{|(2.5-i)|} w & -(l_i) \end{bmatrix}, \forall i = 1, 2, 3, 4$

$\delta_i = 1, i = 1, 4$

$= -1, i = 2, 3$

$\overrightarrow{P}_{og} = \begin{bmatrix} x & y & z \end{bmatrix}$

$\overrightarrow{P}_{oci} = \begin{bmatrix} x_{ci} & y_{ci} & z_{ci} \end{bmatrix}$

R is the rotation matrix describing the orientation of the $\{G\}$ (refer figure 2(a)) with respect to body fixed frame $\{L\}$. We assume the form of R given in [25] for fixed angle representation. $\{G\}$ has the same orientation as the inertial frame $\{0\}$ but moves along with the robot and is attached at the same point as frame $\{L\}$. $(2.5 - i)$ and δ has been incorporated to ensure proper sign of

w and h corresponding to each vertex of the chassis. l_i are the equivalent leg lengths which includes the radius of the wheels. h and w are width and breadth of the chassis.

We linearize the rotation matrix R in (3) by assuming small variation in roll β and pitch γ. Expanding (3), we get the following equations.

$$x_{ci} = x - \frac{2.5 - i}{|(2.5 - i)|} w \sin\alpha - l_i \gamma \sin\alpha + \delta h \cos\alpha - l_i \beta \cos\alpha \tag{4}$$

$$y_{ci} = y + \frac{2.5 - i}{|(2.5 - i)|} w \cos\alpha - l_i \beta \sin\alpha + \delta h \sin\alpha + l_i \gamma \cos\alpha \tag{5}$$

$$z_{ci} = z + \frac{2.5 - i}{|(2.5 - i)|} w\gamma - l_i - \delta h \beta \tag{6}$$

The wheel ground contact points x_{ci}, y_{ci}, z_{ci} would also satisfy the terrain equation (2) and to explicitly solve for β and γ as a function of x, y, α it is required that (2) could be represented as a combination of piecewise linear planes. In case when the fitted terrain equation to the DEM is non-linear we can linearise the terrain equation about the vehicle's geometric centre. This linearisation is justified since any terrain can be locally represented by a linear plane having a particular orientation in 3D space. Linearising (2) about the current chassis centre coordinate gives

$$z_{ci} = k_3 + k_1(x_{ci} - x) + k_2(y_{ci} - y) \tag{7}$$

where $k_3 = g(x, y)$, $k_1 = \frac{\partial(g)}{\partial b}, b = x, c = y$, $k_2 = \frac{\partial(g)}{\partial c}, b = x, c = y$.

Substituting x_{ci}, y_{ci}, z_{ci} values from (4), (5), and (6), four equations represented by (7) can be written in the matrix form as

$$\begin{bmatrix} 1 & w + \eta_1 & h + \nu_1 \\ 1 & w + \eta_2 & -h + \nu_2 \\ 1 & -w + \eta_3 & -h + \nu_3 \\ 1 & -w + \eta_4 & h + \nu_4 \end{bmatrix} \begin{bmatrix} z \\ \gamma \\ \beta \end{bmatrix} = \begin{bmatrix} H_1 \\ H_2 \\ H_3 \\ H_4 \end{bmatrix} \tag{8}$$

η_i, ν_i, H_i are given by the following expressions and are a function of suspension travel length.

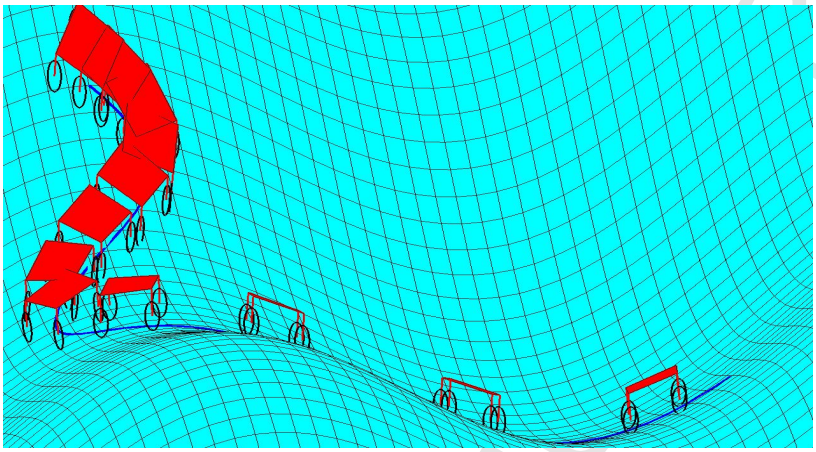

(a)

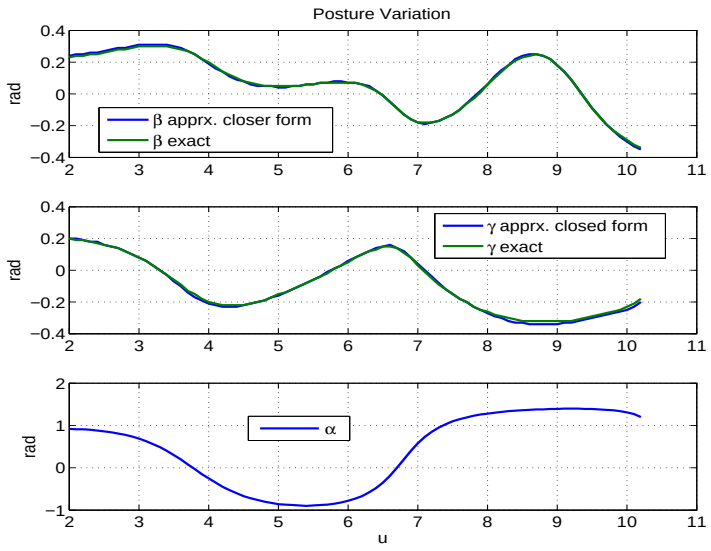

(b)

Figure 3: (a): Vehicle evolution obtained through approximate closed form solutions (b): Posture Variation along the path. The figure shows that the posture obtained through approximate analytical functions agree well with that obtained from solving (3) exactly in the non-linear form through the numerical approach presented in our earlier work [19]. The x axis of the plot shown refers to the arc length "u"

$$\eta_i = k_1 l_i \sin\alpha - k_2 l_i \cos\alpha \quad (9)$$

$$\nu_i = k_1 l_i \cos\alpha + k_2 l_i \sin\alpha \quad (10)$$

$$H_1 = k_1 x - k_1 w \sin\alpha - k_1 h \cos\alpha + k_2 y - k_2 h \sin\alpha + k_2 w \cos\alpha + k_3 + l_1 \quad (11)$$

$$H_2 = k_1 x + w(k_2 \cos\alpha - k_1 \sin\alpha) + h(k_1 \cos\alpha + k_2 \sin\alpha) + k_3 + l_2 + k_2 y \quad (12)$$

$$H_3 = k_1 x + w(k_1 \sin\alpha - k_2 \cos\alpha) + h(k_1 \cos\alpha + k_2 \sin\alpha) + k_3 + l_3 + k_2 y \quad (13)$$

$$H_4 = k_1 x + w(k_1 \sin\alpha - k_2 \sin\alpha) + h(-k_1 \cos\alpha - k_2 \sin\alpha) + k_3 + l_4 + k_2 y \quad (14)$$

The coefficient matrix in (8) can be pseudo-inverted to solve for z, β, γ. However if the suspension travel length is small which essentially means that $\eta_1 = \eta_2 = \eta_3 = \eta_4 = \eta$, and $\nu_1 = \nu_2 = \nu_3 = \nu_4 = \nu$, with small matrix manipulation (8) can be reduced to

$$\begin{bmatrix} 0 & 2w & 0 \\ 0 & 0 & -2h \\ 1 & -w+\eta & h+\nu \end{bmatrix} \begin{bmatrix} z \\ \gamma \\ \beta \end{bmatrix} = \begin{bmatrix} H_2 - H_3 \\ H_3 - H_4 \\ H_4 \end{bmatrix} \quad (15)$$

Inverting coefficient matrix in (15) gives z, γ, β as analytical functions of x, y, α and consequently we obtain the functions $f_1(.), f_2(.)$ and $f_3(.)$. Figure 3(a) shows the 6D evolution of the robot obtained along a path with the analytical functions just derived. Figure 3(b) shows that the posture obtained through approximate analytical functions agree well with that obtained from solving (3) exactly in the non-linear form with the numerical approach presented in our earlier work [19]

3. Dynamics and Stability Constraints

In this section, we make use of the derivations presented in the section 2 to derive the full 3D dynamics of the robot. Considering the scope of motion planning framework discussed in the later sections, the derivation presented in this section, corresponds to a four wheeled robot with non-holonomic kinematics and independent torque actuation at each wheel, similar to the class of electric

vehicles reported in [26]. The evolution model of the considered robot on uneven terrain can thus be described as

$$\begin{cases} \dot{y} = \dot{x}\tan\alpha \\ \dot{z} = \dot{f}_1(x, \dot{x}, \alpha, \dot{\alpha}) \\ \dot{\beta} = \dot{f}_2(x, \dot{x}, \alpha, \dot{\alpha}) \\ \dot{\gamma} = \dot{f}_3(x, \dot{x}, \alpha, \dot{\alpha}) \\ \ddot{x} = U_1 \\ \ddot{\alpha} = U_2 \end{cases} \tag{16}$$

However, it should be noted that the derivations presented in this section can be easily adapted to any four wheeled generic vehicles with independent torque actuation at each wheel. For example, an adaptation of the presented framework has already been reported in our earlier works [14] for all wheel steered vehicles. While adapting the framework to vehicles with different kinematics, only the first line of (16) needs to be changed; the rest of the structure remains the same.

Now, proceeding with the derivation, we first use (4)-(6) to express wheel ground contact points as a function of x, y and α. Wheel ground contact points location are important because they decide surface unit normal at wheel ground contact point $\hat{n}_i$ in the following manner.

$$\hat{n}_i = \begin{bmatrix} n_{xi} & n_{yi} & n_{zi} \end{bmatrix}^T = \begin{bmatrix} \frac{g_x}{\sqrt[2]{g_x^2+g_y^2+g_z^2}} \\ \frac{g_y}{\sqrt[2]{g_x^2+g_y^2+g_z^2}} \\ -\frac{1}{\sqrt[2]{g_x^2+g_y^2+g_z^2}} \end{bmatrix} \tag{17}$$

$g_x = \frac{\partial(g(b,c))}{\partial b}, b = x_{ci}, c = y_{ci}$ $g_y = \frac{\partial(g(b,c))}{\partial c}, b = x_{ci}, c = y_{ci}$, $g_z = 1$

Once the unit normal vectors are calculated the traction force unit vector can be derived with the help of wheel axis unit vector $\hat{\mu}_i$ in the following manner.

$$\hat{t}_i = \frac{\hat{\mu}_i \times \hat{n}_i}{|(\hat{\mu}_i \times \hat{n}_i)|} \tag{18}$$

With the above information the equations of motion can be written as

$$\sum_{i=1}^{4} N_i \hat{n}_i + \sum_{i=1}^{4} T_i \hat{t}_i + m \begin{bmatrix} 0 & 0 & -g \end{bmatrix}^T = \overrightarrow{F} = \begin{bmatrix} F_x & F_y & F_z \end{bmatrix}^T \tag{19}$$

$$\sum_{i=1}^{4} r_i \times N_i \hat{n}_i + \sum_{i=1}^{4} r_i \times T_i \hat{t}_i = \overrightarrow{M} = \begin{bmatrix} M_x & M_y & M_z \end{bmatrix}^T \tag{20}$$

$$r_i = \overrightarrow{P}_{gci} \tag{21}$$

$$F_x = ma_x \tag{22}$$

$$F_y = ma_y \tag{23}$$

$$F_z = ma_z \tag{24}$$

$$M_x = I_{xx}\dot{\Omega}_x + I_{zz}\Omega_y\Omega_z - I_{yy}\Omega_y\Omega_z \tag{25}$$

$$M_y = I_{yy}\dot{\Omega}_y + I_{xx}\Omega_x\Omega_z - I_{zz}\Omega_x\Omega_z \tag{26}$$

$$M_z = I_{zz}\dot{\Omega}_z + I_{yy}\Omega_x\Omega_y - I_{xx}\Omega_x\Omega_y \tag{27}$$

In (19), g is the magnitude of acceleration due to gravity, while, I_{xx}, I_{yy}, I_{zz} in (25)-(27) are the moment of inertia of the chassis and here a diagonal Inertia matrix has been taken.

Equations (19) and (20) can be written in the following matrix form

$$A * C = D \tag{28}$$

where $C = \begin{bmatrix} T_i & N_i \end{bmatrix}^T_{2n\times 1}$ $D = \begin{bmatrix} m\overrightarrow{a} & I\dot{\overrightarrow{\Omega}} + \overrightarrow{\Omega} \times I\overrightarrow{\Omega} \end{bmatrix}^T_{6\times 1}$ T_i,N_i,$\overrightarrow{a}$,$\dot{\overrightarrow{\Omega}}$, $\overrightarrow{\Omega}$ are the traction, normal forces, linear and angular acceleration and angular velocity respectively. n is the number of wheels of the vehicle, m is the mass of the vehicle and $I_{3\times 3}$ is the inertia matrix. The elements of $A_{6\times 2n}$ matrix depends on vehicle posture, geometry and terrain dependent parameters like surface

contact normal and traction unit vectors. It is to be noted that because of the derivation presented from (4-15), matrix A can also be known in closed form as a function of x, y, α. Inverting the matrix A results in the following expressions, relating traction and normal forces to the terrain's geometry, robot's state and control inputs.

$$T_i = a_{i1}(ma_x) + a_{i2}(ma_y) + a_{i3}(mg + ma_z) + a_{i4}(I_{xx}\dot{\Omega}_x + I_{zz}\Omega_y\Omega_z - I_{yy}\Omega_y\Omega_z) + a_{i5}(I_{yy}\dot{\Omega}_y + I_{xx}\Omega_x\Omega_z - I_{zz}\Omega_x\Omega_z) + a_{i6}(I_{zz}\dot{\Omega}_z + I_{yy}\Omega_x\Omega_y - I_{xx}\Omega_x\Omega_y) \quad (29)$$

$$N_i = a_{j1}(ma_x) + a_{j2}(ma_y) + a_{j3}(mg + ma_z) + a_{j4}(I_{xx}\dot{\Omega}_x + I_{zz}\Omega_y\Omega_z - I_{yy}\Omega_y\Omega_z) + a_{j5}(I_{yy}\dot{\Omega}_y + I_{xx}\Omega_x\Omega_z - I_{zz}\Omega_x\Omega_z) + a_{j6}(I_{zz}\dot{\Omega}_z + I_{yy}\Omega_x\Omega_y - I_{xx}\Omega_x\Omega_y) \quad (30)$$

$\forall\ i = \{1, 2, 3, 4\}$, $\forall\ j = i + 4$. The term g is the acceleration due to gravity. The coefficients a_{i1},a_{i3},a_{j2}..a_{in},a_{jn}, are the elements of the pseudo inverse of matrix A and $a_x = \ddot{x}, a_y = \ddot{y}, a_z = \ddot{z}$. The coefficients of the pseudo inverse matrix depends explicitly on the terrain conditions and the terrain geometry.

The permanent contact and no-slip constraints can be written in terms of traction and normal forces at the wheel ground contact points through the following relations.

$$N_i > 0 \quad (31)$$

$$|(T_i)| < \rho N_i \Rightarrow -T_i \leq \rho N_i, T_i \leq \rho N_i \quad (32)$$

$$\mathbf{C}(\mathbf{X}, \dot{\mathbf{X}}, \mathbf{U}) = \begin{cases} -N_i < 0 \\ -T_i \leq \rho N_i, T_i \leq \rho N_i \end{cases} \quad (33)$$

In (32), ρ is the coeffecient of friction. It is straightforward to understand that if matrix A could be inverted symbolically, we could have analytical functional description of constraints (33) and in theory we could have a gradient descent based algorithm to generate a one shot stable trajectory. However,

robots operating on uneven terrain generally have 4-8 wheels which makes A under-constrained and have to be pseudo-inverted. Some algorithms like [27] computes symbolic pseudo inverse for small matrices having one or two independent variables. However pseudo-inverting matrix A, whose dimension will increase with the number of wheels can turn into a complex problem. It should be noted that this problem is not unique to the framework proposed in this paper but is fundamental with modelling robot dynamics in 3D and relating traction and normal forces to velocity and acceleration in closed form. This is a fundamental bottleneck associated with using permanent contact and no-slip as stability constraints. In contrast, constraints resulting from *tip-over* stability [4], [5] have an analytical form and hence is easier to incorporate in motion planning. But as mentioned earlier, this increase in complexity resulting from the use of permanent contact and no-slip constraints is essential for accurate motion planning on uneven terrain.

4. Solution Space of the differntial stability constraints

The variable in the differential stability constraints (33) are the control inputs. Recall from (16) that we take acceleration as the control input. Thus, we are interested in obtaining the space of feasible/stable accelerations satisfying the constraints (33) for a given state of the robot. We next present a method for obtaining the feasible set of accelerations. We then describes how this feasible set can itself act as a stability metric.

4.1. Obtaining Feasible/Stable Set of Accelerations

As shown in (16), the control input is taken as the acceleration pair $(\ddot{x}, \ddot{\alpha})$. To obtain the feasible set of accelerations at any given state, we search $\ddot{x}$ in the range $(\ddot{x}_{max}, \ddot{x}_{min})$ and $\ddot{\alpha}$ in the range $(\ddot{\alpha}_{max}, \ddot{\alpha}_{min})$ to find those values which satisfy (33). In other words, we generate a fixed grid of values for $\ddot{x}$ and $\ddot{\alpha}$ and ascertain which of the grid point values satisfy the constraints. Here the subscript *min* and *max* stands for maximum negative and positive accelerations

respectively. We refer to the number of discrete feasible acceleration pairs at a given state as the *feasible acceleration count* (*FAC*).

For a non-holonomic robot, the control input is usually body frame aligned acceleration $\dot{v}$ and not the $\ddot{x}$. However, these two are related in the following manner.

$$(\ddot{x}, \ddot{y}, \ddot{z})^T = R \begin{bmatrix} 0 & \dot{v} & 0 \end{bmatrix}^T + \dot{R} \begin{bmatrix} 0 & v & 0 \end{bmatrix}^T \tag{34}$$

In (34), v is the robot velocity in the body/local reference frame. Due to the non-holonomic constraint v and $\dot{v}$ are assumed to align with the robot longitudinal axis in the robot's body/local frame. Now with the help of the evolution model (16) and the derivations presented in section 2, at every state of the robot, we can compute the space $(\ddot{x}_{max}, \ddot{x}_{min})$ corresponding to space of actual control input $(\dot{v}_{max}, \dot{v}_{min})$. The process of obtaining the feasible acceleration set can then be performed as described above.

4.2. Physical Significance of Feasible Acceleration Count (FAC) from Stability and Motion Planning Point of View

Maneuver at a given state is dictated by the control input which in our case is the acceleration. Thus, encodes the ability of the robot to perform various set of motions at given state and can be used as a metric to describe how stable the robot is on the terrain. Alternatively, it can be viewed as the set of discrete control inputs available for expansion of the tree in the sampling based planners like RRT. As the state of the robot evolves on the uneven terrain, *FAC* and consequently the set of feasible control inputs would change. The number of available control inputs directly affects the quality of state-space exploration. Thus, it can be seen that there is a direct co-relation between the quality of stability and maneuverability of the robot as defined by *FAC* and quality of state space exploration achieved at each step of incremental sampling based planners like RRT. Deducing this co-relation is one of the important contribution of the proposed work. In the light of this information, we next summarize the proposed incremental trajectory planner for motion planning on uneven terrain.

5. Incremental Trajectory Generation on Uneven Terrain

The proposed incremental trajectory planner has a data structure similar to (RRT) [1]. However in contrast to the general RRT framework [1], it has an additional step for computing the space of feasible control input. Further, a novel node selection criteria is introduced for the expansion of the tree.

Step 1

For the current state of the robot $(x, y, z, \alpha, \beta, \gamma, \dot{x}, \dot{y}, \dot{z}, \dot{\alpha}, \dot{\beta}, \dot{\gamma})$, search for $\ddot{x}$ in the range $(\ddot{x}_{max}, \ddot{x}_{mins})$ and $\ddot{\alpha}$ in the range $(\ddot{\alpha}_{max}, \ddot{\alpha}_{min})$ to find n discrete values satisfying the stability constraints (33). The evolution model (16) is integrated for a short duration of time with n feasible control inputs to obtain n next instant state.

Step 2

For the n number of states resulting from the forward evolution described above, the following metric is evaluated

$$M = \frac{FAC}{d}. \tag{35}$$

where d represents the geodesic distance to the goal. A state which maximises the metric M is chosen and updated as the current state. Metric M is maximised when FAC is maximised and distance to the goal is minimized. The step 1 and 2 are repeated till the robot reaches the goal configuration.

To understand the motivation and necessity for the proposed node selection criteria, note that the node selection criteria for a general RRT framework [1] involves computing the distance of the all the current nodes of the tree with a randomly selected configuration. The node which has the minimum distance is selected for expansion and the iteration continues. Since the random configuration can be chosen from the obstacle free work space, it automatically satisfies the geometric obstacle avoidance constraints. But unlike indoors where obstacles are vertical projections from a horizontal ground plane and all obstacles

need to be strictly avoided, in outdoors the distinction between obstacles and ground is hazy as the obstacles and ground blend with each other to form the terrain. As such an obstacle free configuration has little physical significance. On uneven terrains, stability and maneuverability is far more generic concept. If the robot can maneuver with stability over a part of the terrain, then that part is not an obstacle and vice versa. But it is difficult to ascertain the stability of a configuration as the stability constraints depend on both state and the control input. Thus the proposed metric M is an apt choice for node selection criteria as it captures the stability and maneuverability of robot's state corresponding to a particular node in a tree. Moreover, as discussed in the previous section, FAC decides the quality of state space exploration and hence maximising FAC would ensure better efficiency of the proposed incremental trajectory planner.

Figure 4 illustrates couple of steps of the proposed incremental trajectory planner. Four feasible control inputs are obtained at the first step. The forward evolution model is integrated for a short duration of time with these four control inputs, resulting in construction of a tree where the number of branches is equal to the number of feasible control inputs obtained. Out of the four states resulting from the integration of the evolution model, the one shown in blue has the highest value for M. Hence, this particular state is chosen and updated as the current state and the process is repeated. As evident from the figure, that the number of available control inputs for the construction of tree at each iteration would vary as the state of the robot evolves on the uneven terrain. In particular, it can be seen that only three feasible control inputs (and consequently three branches) are obtained at the second iteration as compared to four, obtained at the first iteration.

6. Simulation Results

The objective of this section is two fold : Firstly, to highlight the efficacy of the proposed incremental trajectory planner in generating trajectories satisfying stability constraints (33). In particular, we highlight the effect that the metric

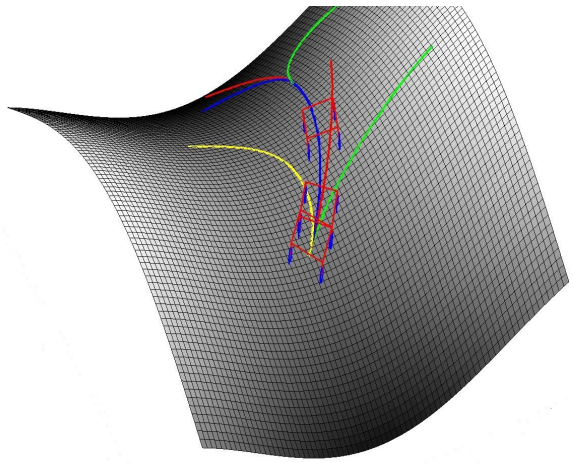

Figure 4: Iterations of the proposed incremental trajectory planner. As can be seen that the number of control inputs available for the construction of tree at each iteration varies as the state of the robot evolves on the uneven terrain.

M has on trajectory produced by incremental sampling based planners. Secondly, to show the effectiveness of *Feasible Acceleration Count* (FAC) as a combined measure of robot's maneuverability and stability. In the simulations, we consider a small robot of dimension $1.2 \times 1.2 \times 1.2$ m^3 and mass $m = 10kg$ in the simulation. The model of the uneven terrain had the form $A\sin(ax) + B\cos(by)$. Terrains with different geometry were generated by changing the coefficients of the terrain model. The friction coefficient between the robot wheels and the terrain, ρ was kept at 0.7. The proposed incremental planner was required to generate trajectories between a start and a goal position. The final heading and velocities were considered free. The feasible $\ddot{x}$ and α and consequently FAC was obtained by searching in a 100 X 100 grid

We first present motion planning results for a generic four wheeled mobile robot on uneven terrain. We then extend the proposed trajectory planner, the concept of FAC and cost metric M to articulated robotic systems like a mobile manipulator. We show that by just expanding the state space, all of the concepts described till now can be naturally applied for motion planning of high-dof systems like mobile manipulators on uneven terrain.

6.1. Effect of Metric M on Motion Planning on Uneven Terrains

In this section, we highlight how the metric proposed in (35) influences trajectory generation on uneven terrain. For this purpose, two sets of trajectories as shown in figure 5(a)-5(b) were computed. The first set of trajectories (shown in green) maximizes the metric M of (35), while the trajectories shown in blue are biased by only the distance to the goal. The variation of FAC along both sets of trajectories are shown in the figures 5(c)-5(d). For the sake of presentation in the plots, we normalise FAC with that obtained on the flat terrain to obtain a number between 0 and 1.It can be seen from these figures that while distance only metric results in shorter trajectories, metric M based trajectories are more stable in terms of FAC. In particular, note the highlighted portions in figures 5(c) and 5(d). FAC along trajectories biased by only the distance to the goal, gets very close to zero. In contrast, optimization of metric M at each instant of the robot's motion ensures that FAC remains well above zero. As stated high FAC signifies high stability and maneuverability and this can be also be inferred by the fact that the FAC trajectories are better aligned with the gradient of the terrain.

It can be easily noted that the proposed incremental planner based on metric M is greedy in nature. It finds the node that maximises M for the next instant. However, the planner does not include information ahead of the immediate next instant nodes. In that sense, while the planner with metric M would move to the node with a higher FAC for the next instant when compared with distance only metric, this action need not always result in globally higher FAC when compared with distance only metric based trajectories. For example, consider figure 5(d) where towards the end, the FAC along distance biased trajectories is more than that obtained along metric M biased trajectories. However, in spite of this limitation, we have observed in simulations that on an average metric M based trajectories ensures far higher FAC than trajectories biased by only the distance to the goal. This is because as explained in the previous sections, FAC directly quantifies the efficiency of the state space and thus, metric M biased incremental planners can perform better exploration of the state space

and thus, is more likely to converge faster to the goal.

6.2. Choice of FAC *Vs* Tip-Over *Metric for Motion Planning on Uneven Terrains*

Figure 6(a)-7(d) show the trajectories generated on uneven terrain between four different start and goal locations. Two kinds of trajectories were generated in each example. The first set of trajectories ($\mathbf{X}_{F0}$, $\mathbf{X}_{F1}$, $\mathbf{X}_{F2}$, $\mathbf{X}_{F3}$) shown in red result from using stability constraints presented in (33) which enforces the requirement of permanent contact and no-slip at the wheel ground contact points. Consequently, these set of trajectories use metric M as given in (35) as the node selection criteria. The second set of trajectories ($\mathbf{X}_{T0}$, $\mathbf{X}_{T1}$, $\mathbf{X}_{T2}$, $\mathbf{X}_{T3}$) shown in blue are obtained by considering the constraints resulting from the *tip-over* stability concept[4] . The node selection criteria for constructing these trajectories was obtained by modifying the cost metric as $M = \frac{tip-over-margin}{d}$. Thus, the trajectories shown in red seek to optimize FAC at each iteration of the trajectory planner, while the trajectories shown in blue optimize the tip-over stability. A common pattern that emerges out of all the four examples 6(a)-7(d) is that the tangent to the FAC based trajectories aligns better with the gradient of the terrain than the tip-over based trajectories. Since the tangent to the trajectory would correspond to the robot heading, FAC based trajectories would encourage robot to move along the gradient. It can be intuitively reasoned that it is easier to maneuver while moving along the gradient of the terrain than across it. Thus the behavioral differences between the FAC and tip-over based trajectories further strengthens the discussion of section 1.1: tip-over stability does not capture the ability of the robot to execute various motions and is not suitable for motion planning on uneven terrain. FAC on the other hand has been carved out specifically for motion planning and can act as the combined measure of maneuverability and stability. To further quantitatively justify this claim, two sets of simulations were performed. We evaluated the tip-over margin along the FAC based trajectories, $\mathbf{X}_{F0}, \mathbf{X}_{F1}, \mathbf{X}_{F2}, \mathbf{X}_{F3}$ and FAC along the tip-over based trajectories $\mathbf{X}_{T0}, \mathbf{X}_{T1}, \mathbf{X}_{T2}, \mathbf{X}_{T3}$. The results are summarized

in figure 8(a)-8(d). For the sake of comparison, we normalise FAC and tip-over margin by the values obtained on the flat terrain and thus they appear in the plots as non-dimensional number between 0 and 1. It can be seen from the figures that FAC based trajectories also ensures that the tip-over stability constraints are satisfied. However, the converse is not true as FAC goes to zero at various places along the trajectories based on tip-over stability constraints.

Figure 9(a)-9(d) show the variation of robot's roll, β, pitch, γ and z co-ordinate of the robot along the FAC based trajectories, $\mathbf{X}_{F0}$, $\mathbf{X}_{F1}$, $\mathbf{X}_{F2}$ and $\mathbf{X}_{F3}$. It can be seen that the plots further validate the approximate closed form evolution model derived in section 2. On moderately uneven terrains, baring a few isolated points, the evolution obtained through approximate model agrees well with that obtained from solving the non-linear model (3) exactly through numerical means. At this point, it is worth mentioning that on more complex terrains, one could easily resort to exact numerical solution of (2) for deducing the evolution of 6D pose of the robot. Use of numerical solution over approximate closed form solution, does not in any way affect the framework described in this paper. To be precise, the derivation of dynamics, the concept of FAC and the incremental motion planning framework holds as such with numerical solution approach as well. A preliminary implementation with numerical solution approach can be found in earlier work [19].

Figure 10(a)-11(d) validates the satisfaction of permanent contact and no-slip constraints, (33) along the FAC based trajectories.

6.3. Motion Planning for Mobile Manipulators on Uneven terrain.

In this section, we consider the problem of coordinating the motion of the manipulator and the robot base when the manipulator is not constrained to follow any trajectory. Similar to the previous section, the objective still remains to generate feasible/stable trajectories for the robot base between a given start and a goal location. However, now appropriate motions for the additional *dofs* of the manipulator also needs to be planned so that the combined system can navigate without loosing stability on uneven terrain. These kind of situations

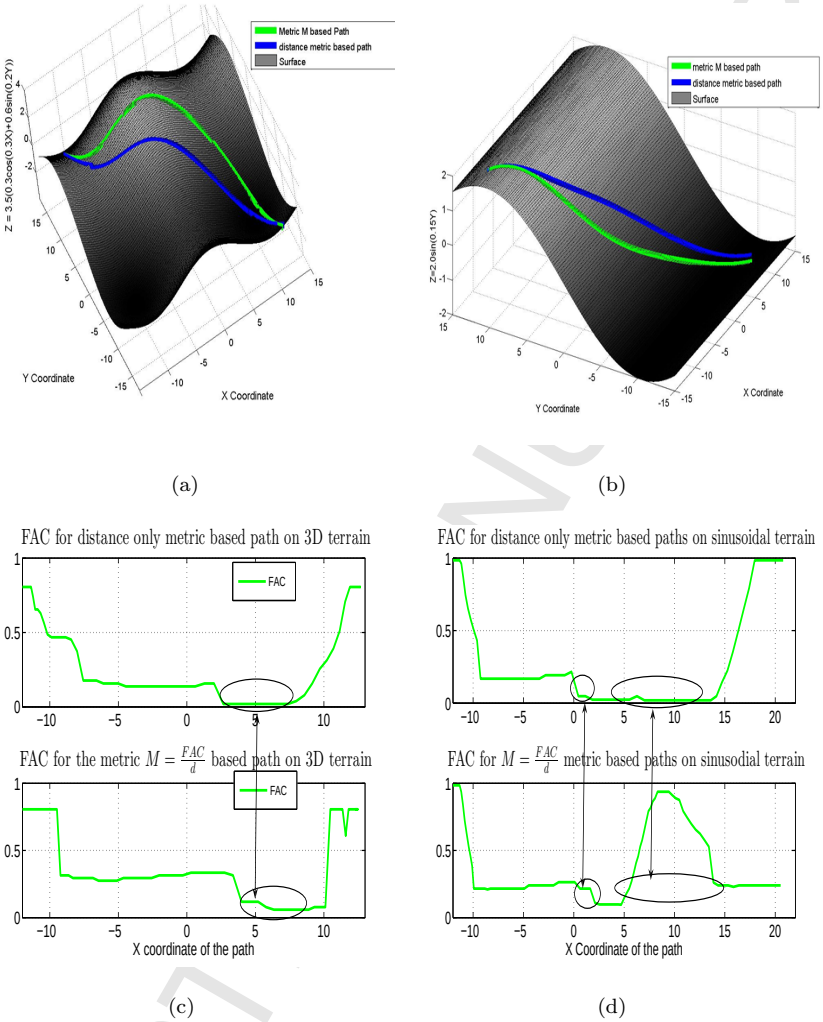

Figure 5: (a)-(d): Influence of the proposed node selection metric M on trajectory generation on uneven terrains. It can be seen from the figures (a) and (b) that the incremental trajectory planner biased by only distance to the goal produces shorter trajectories. In fact, the distance biased trajectories actually cuts across the gradient of the terrain. In contrast, the trajectory planner biased by the metric M aligns itself with the gradient of the terrain. While, this increases the trajectory length, it also ensures a higher stability. The stability of the robot as measured by FAC for distance only and metric M based trajectories are shown in (c) and (d). It is easy to observed that FAC for distance biased trajectories gets very close to zero, while in contrast, metric M biased trajectories enjoy FAC well above zero.

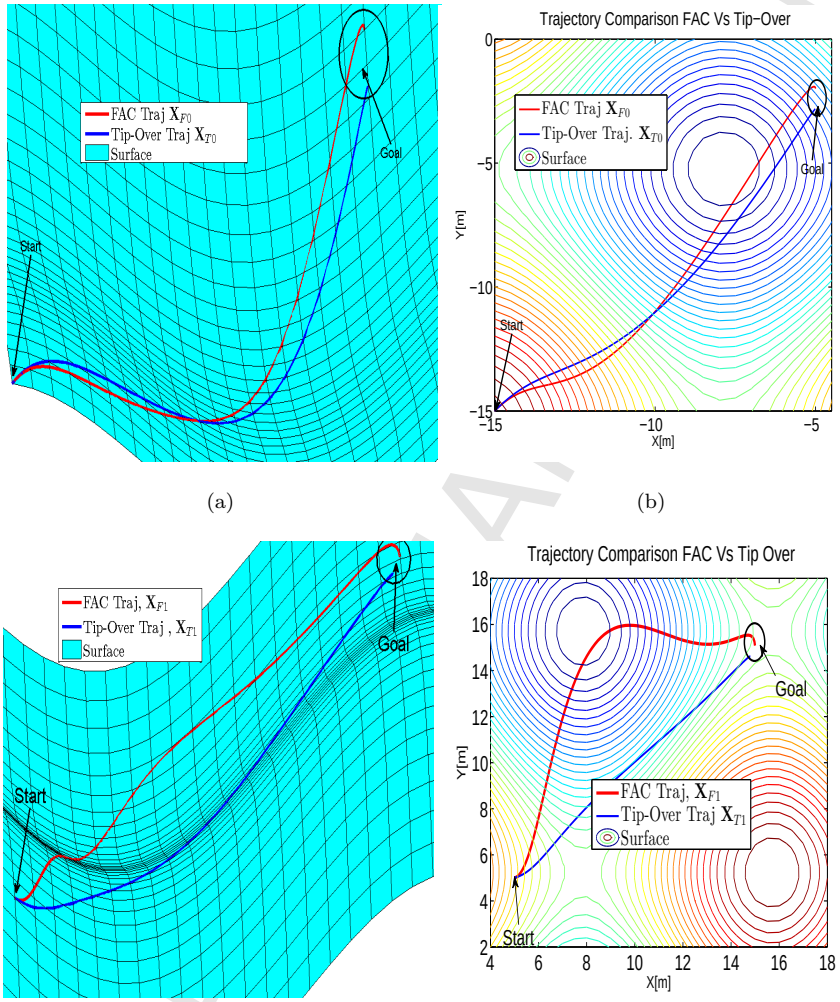

Figure 6: Trajectories X_{F0}, X_{F1} produced by the incremental sampling based planners with metric $M = \frac{FAC}{d}$. These trajectories are compared with X_{T0}, X_{T1} produced by the planner with metric $M = \frac{tip-over-margin}{d}$. It can be clearly seen that FAC based trajectories are better aligned with the gradient of the terrain, thus allowing for better maneuverability.

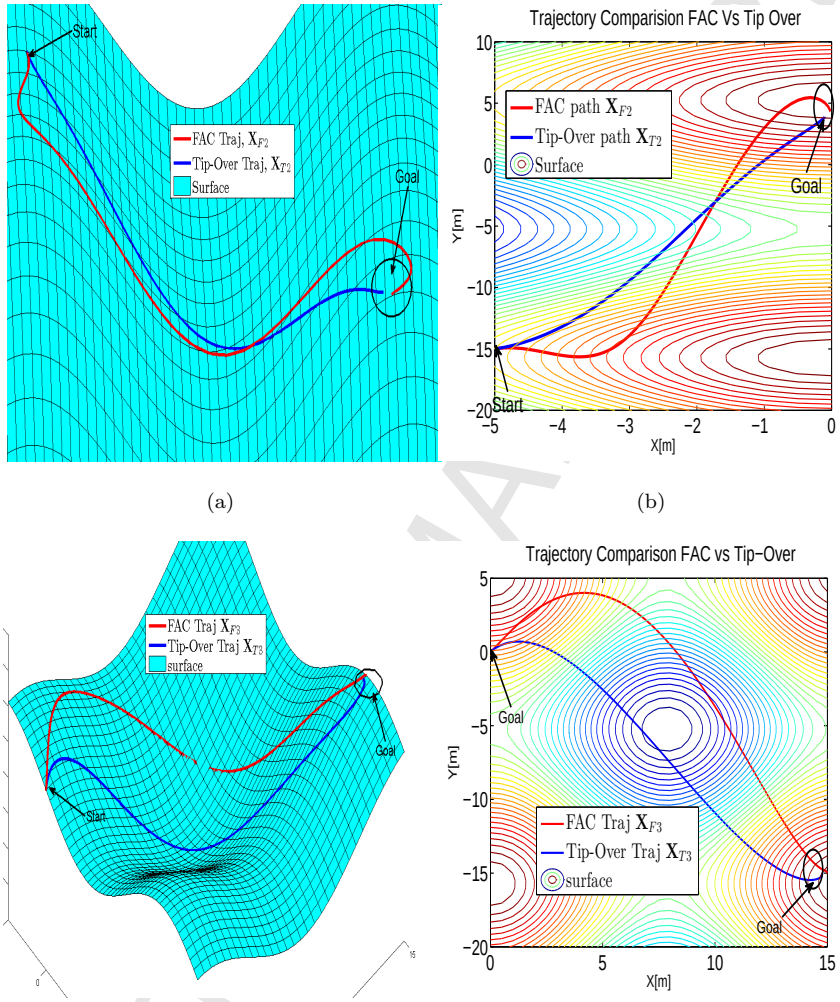

Figure 7: Similar results as that presented in figures 6(a)-6(d). Again, it can be seen that FAC based trajectories X_{F2} and X_{F3} are better aligned with gradient of the terrain that tip-over margin based trajectories X_{T2} and X_{T3}

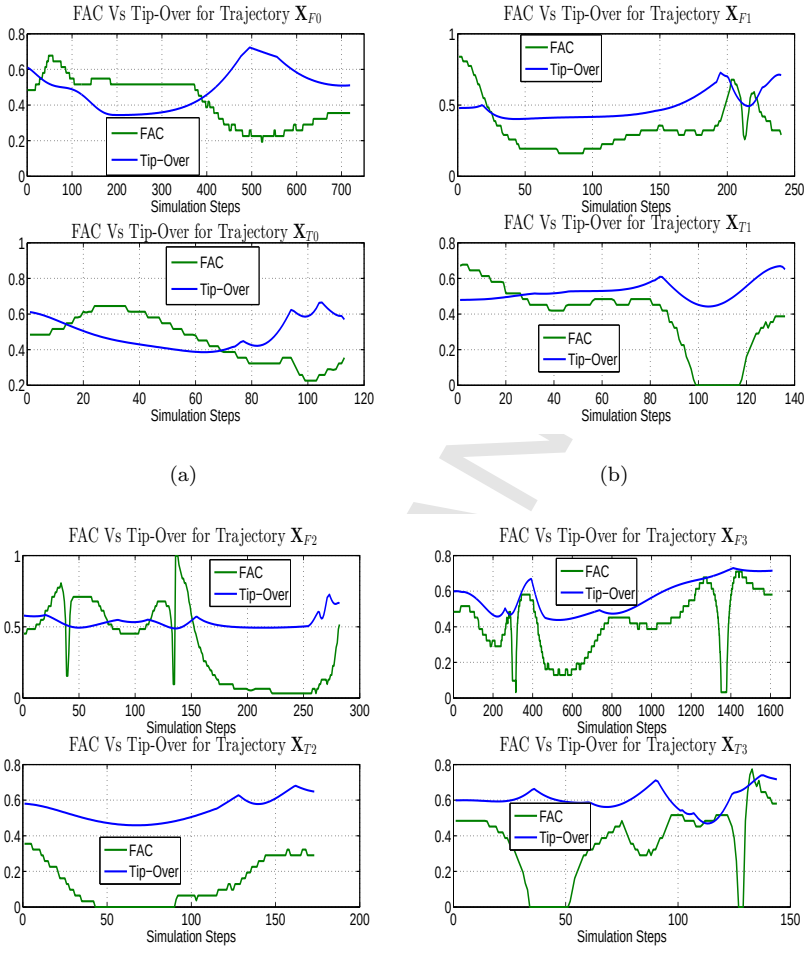

Figure 8: (a)-(d): Quantitative Comparison of FAC with *tip-over* stability metric. Both FAC and *tip-over* margin were evaluated along the trajectories, $\mathbf{X}_{F0}$, $\mathbf{X}_{F1}$, $\mathbf{X}_{F2}$, $\mathbf{X}_{F3}$ obtained through FAC and the trajectories $\mathbf{X}_{T0}$, $\mathbf{X}_{T1}$, $\mathbf{X}_{T2}$, $\mathbf{X}_{T3}$ obtained through *tip-over*. It can be seen that FAC trajectories ensures that the *tip-over* margin also remains above zero. However the same conservativeness is not shown by *tip-over* trajectories as FAC goes to zero at various points along the tip-over trajectories. This experiment further strengthens the position of FAC as a combined measure of manoeuvrability and stability.

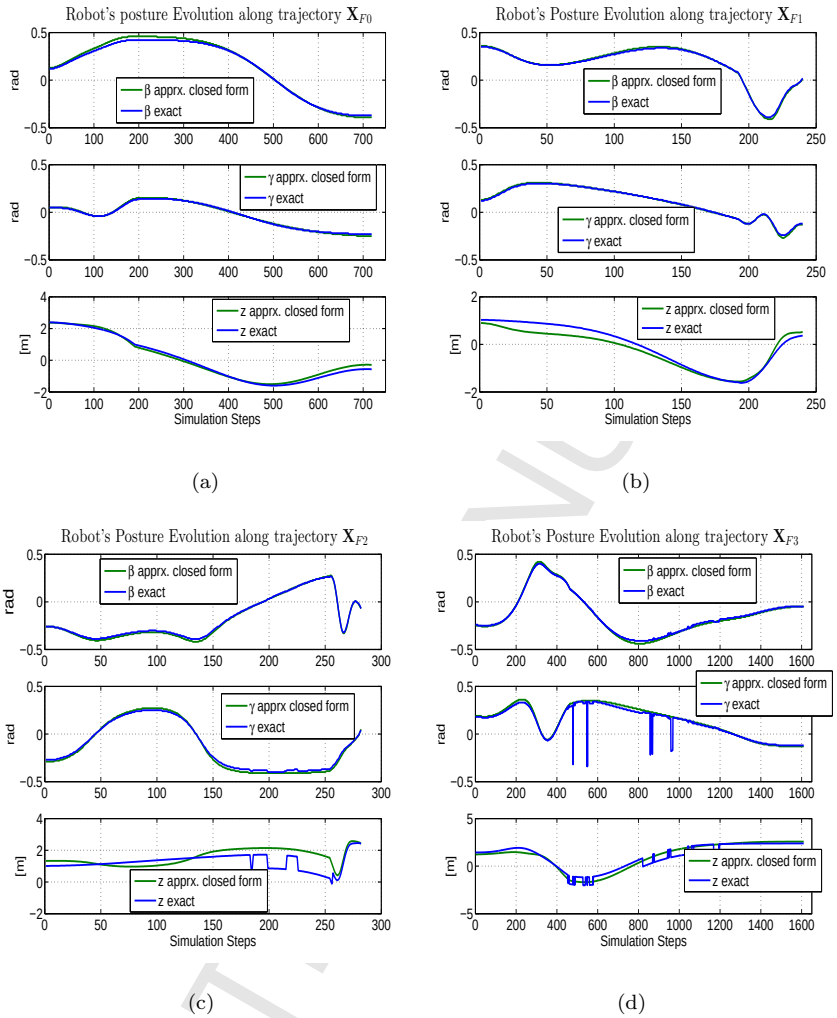

Figure 9: (a)-(d) Posture variation along the *FAC* trajectories. It can be again seen that the approximate closed form evolution model agrees well with the exact non-linear evolution model.

often arise in planetary exploration, where rovers equipped with a manipulator are required to navigate over general uneven terrain. Moreover the framework can also be used in situations where the mobile manipulator is required to transport objects on uneven terrain, [28]. The generated trajectories seek to maximize the *FAC* for the combined robot and manipulator system.

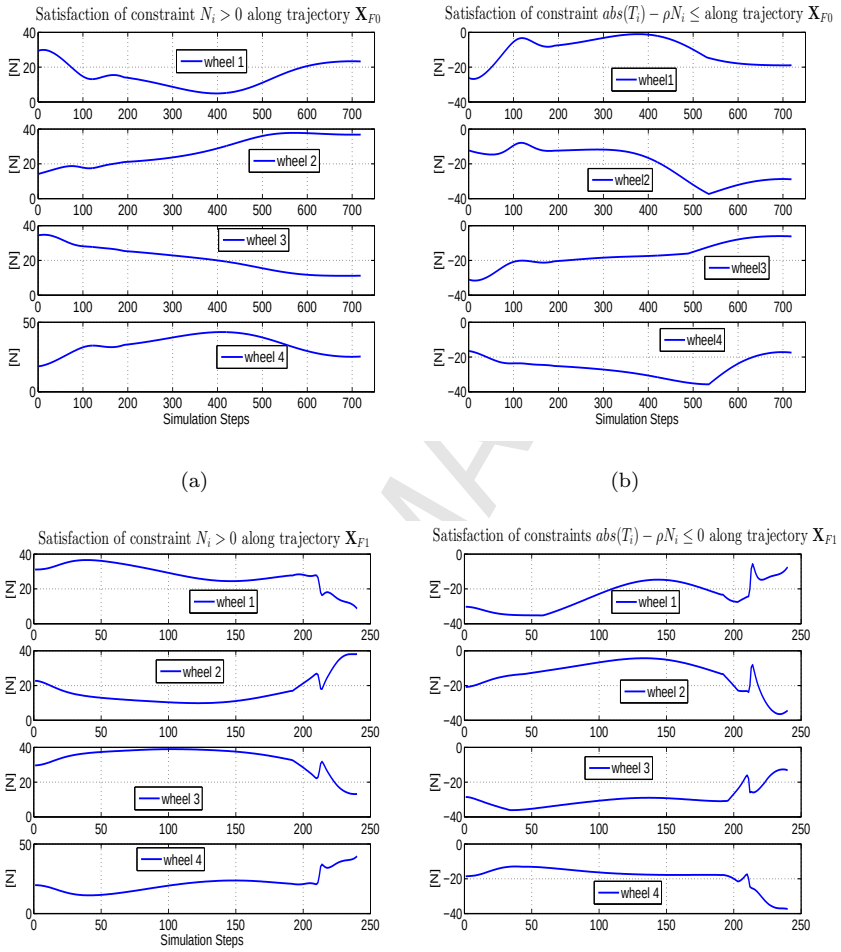

Figure 10: Satisfaction of permanent contact constraint ($N_i > 0$) and no-slip constraint ($|T| - \rho N_i \leq 0$) along FAC based trajectories X_{F0} and X_{F1}

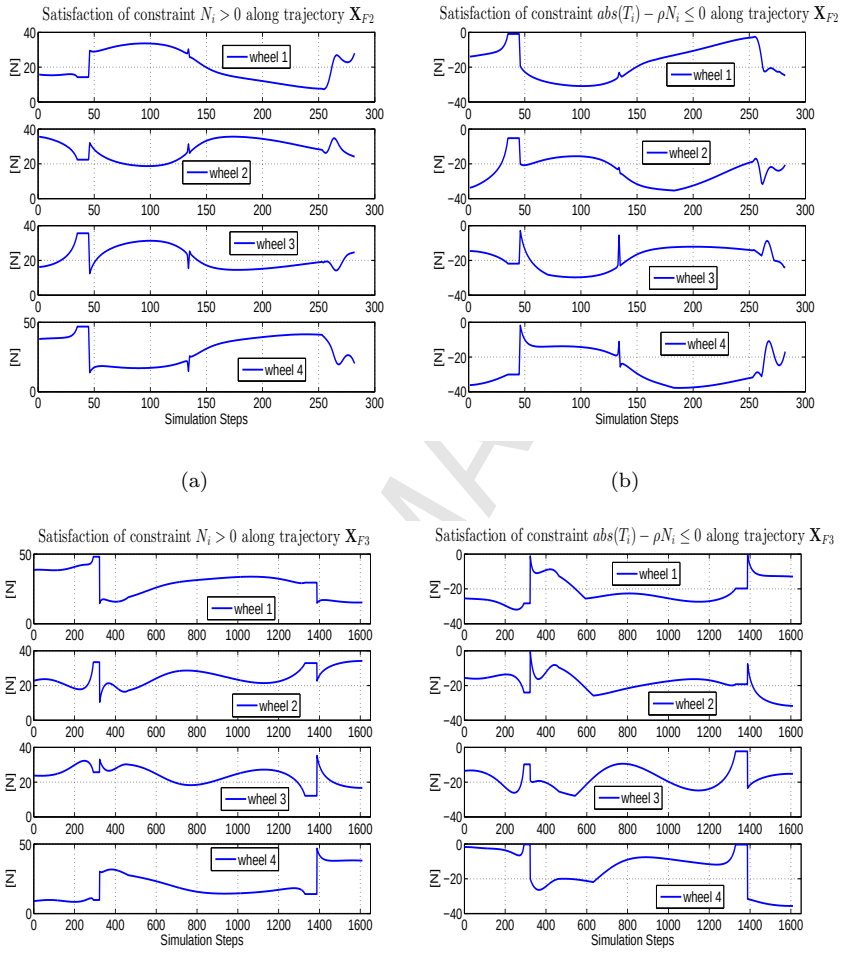

Figure 11: Satisfaction of permanent contact constraint ($N_i > 0$) and no-slip constraint ($|T| - \rho N_i \leq 0$) along FAC based trajectories X_{F2} and X_{F3}

The problem of coordinating the motion of the robot base and the manipulator has been previously addressed in works like [5], [29], [30], . A two level approach has been adopted in these cited works, where at the first level a path is computed in the configuration space and then at the second level an appropriate time parametrization of the paths are obtained considering the effect of manipulator dynamics. These approaches suffer from the drawback that the configuration space planning needs to be repeated if there exists no feasible velocity and acceleration between two points, which as already shown in the previous section, could indeed often be the case on uneven terrains. Authors in [31], [32] address a relatively simpler problem of analysing the mobile manipulator stability for a given trajectory of robot base and manipulator. But since they do not provide any framework for computing the general 6 *dof* evolution of the robot base, extending their method to a more general planning domain would be difficult. The current paper proposes an unified approach of simultaneous motion planning of robot base and manipulator on uneven terrain.

The approach can be naturally built on the concepts discussed till now by just expanding the configuration space and control input space to include the manipulator joint variables. The configuration space and control input space of the mobile manipulator would have the following form

$$\mathbf{X}_{man} = (x, y, z, \alpha, \beta, \gamma, \phi_i)^T, \mathbf{U}_{man} = (\ddot{x}, \ddot{\alpha}, \ddot{\phi_i}), \forall i = 1, 2...p \tag{36}$$

where ϕ_i are the manipulator joint angles and p is the number of joints in the manipulator. The expansion in the configuration and control input space induces the following changes in the expression for traction and normal forces.

$$\begin{aligned} T_i = a_{i1}(ma_x + F_{0x}) + a_{i2}(ma_y + F_{0y}) + a_{i3}(mg + ma_z + F_{0z}) \\ +a_{i4}(I_{xx}\dot{\Omega}_x + I_{zz}\Omega_y\Omega_z - I_{yy}\Omega_y\Omega_z + M_{0x}) \\ +a_{i5}(I_{yy}\dot{\Omega}_y + I_{xx}\Omega_x\Omega_z - I_{zz}\Omega_x\Omega_z + M_{0y}) \\ +a_{i6}(I_{zz}\dot{\Omega}_z + I_{yy}\Omega_x\Omega_y - I_{xx}\Omega_x\Omega_y + M_{0z}) \end{aligned} \tag{37}$$

$$
\begin{aligned}
N_i = a_{j1}(ma_x + F_{0x}) + a_{j2}(ma_y + F_{0y}) + a_{j3}(mg + ma_z + F_{0z}) \\
+a_{j4}(I_{xx}\dot{\Omega}_x + I_{zz}\Omega_y\Omega_z - I_{yy}\Omega_y\Omega_z + M_{0x}) \\
+a_{j5}(I_{yy}\dot{\Omega}_y + I_{xx}\Omega_x\Omega_z - I_{zz}\Omega_x\Omega_z + M_{0y}) \\
+a_{j6}(I_{zz}\dot{\Omega}_z + I_{yy}\Omega_x\Omega_y - I_{xx}\Omega_x\Omega_y + M_{0z}) \qquad (38)
\end{aligned}
$$

where $\overrightarrow{F}_0 = \mathcal{G}_1(x, y, \alpha, \phi_i, \dot{\phi}_i, \ddot{\phi}_i)$ and $\overrightarrow{M}_0 = \mathcal{G}_2(x, y, \alpha, \phi_i, \dot{\phi}_i, \ddot{\phi}_i)$ are the reaction forces exerted by the manipulator on the robot's chassis in the global frame. The functions $\mathcal{G}_1(.)$ and $\mathcal{G}_2(.)$ can be obtained by Newton-Euler formulation which involves computing the linear and angular velocities of each link recursively through outward iterations starting from the base link and then with its help, computing the forces and moments at each link through inward iterations starting from the last link. The equation for recursively computing the velocity, acceleration, forces and moments is given by [25]. Note that the effect of robot's base motion on manipulator dynamics is taken into account by superimposing its motion on the base link of the manipulator during outward iterations. Corresponding to (37) and (38), a feasible acceleration would now be defined as a tuple $(\ddot{x}, \ddot{\alpha}, \ddot{\phi}_i)$ which satisfies the stability constraints (33). Consequently feasible acceleration count, FAC is expanded to include the manipulator accelerations.

In order to perform motion planning for the mobile manipulator system in the same manner as presented for the four wheeled robot in the previous section, the proposed incremental trajectory planner is applied with the expanded configuration and control input space. The stability constraints would have the modified expression for traction and normal forces and the cost metric M now depend on the manipulator accelerations as well. The model of the mobile manipulator used in the simulation is shown in figure 12. The manipulator consists of a 2 *dof* arm. The D-H parameters and inertial properties of the manipulator are summarized in tables 1 and 2 respectively and are taken from our earlier work [20]. Further, the simulation results presented in the subsequent sections are derived from [20]. However, we present a much broader analysis as compared

to [20]. The feasible tuple $(\ddot{x}, \ddot{\alpha}, \ddot{\phi_1}, \ddot{\phi_2})$ and consequently FAC was obtained by searching in a grid of 100 X 100 X 100 X 100 points.

The simulation consists of the following major parts: (i). Comparisons of the trajectories obtained for the robot plus manipulator system and only robot base in terms of FAC to analyze the effect of manipulator motion on stability (ii). Analysis of the manipulator and robot base motion . (iii). Comparison of stability of the mobile manipulator from the viewpoint of tip over margin and FAC.

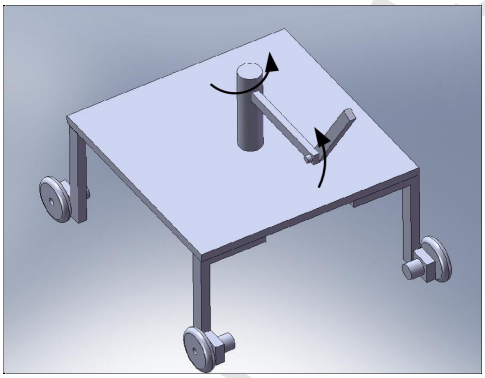

Figure 12: Model of mobile manipulator used in the simulation. It comprises of a base of a generic wheeled mobile robot with a two *dof* non-planar arm.

Table 1: D-H Parameter of the Manipulator

Joint	α_{i-1}	a_{i-1}	d_i	ϕ_i
1	0	0	d_1	ϕ_1
2	$\frac{pi}{2}$	l_1	0	ϕ_2
3	0	l_2	0	0

6.3.1. Comparison of Robot plus Manipulator and only Robot's Motion in terms of FAC

Figure 13(a) shows the final trajectories on uneven terrain. Two trajectories $\mathbf{X}_{m0}$, $\mathbf{X}_{m1}$ are generated for the mobile manipulator starting from the

Table 2: Inetial Properties of the manipulator

Link	$I_{xx}(kg-m^2)$	$I_{yy}=I_{zz}(kg-m^2)$	$mass(kg)$	$d_i(m)$	$l_i(m)$
1	$75*10^-6$	$2.5*10^-3$	0.5	0.40	0
2	$75*10^-6$	$2.5*10^-3$	0.5	0	0.75
3	$75*10^-6$	$2.5*10^-3$	0.5	0	0.75

same initial robot base configuration but different manipulator configuration. A trajectory for only the robot base without the manipulator is also planned for comparative purposes which will be referred to as $\mathbf{X}_v$. The trajectory $\mathbf{X}_v$ is significantly different from $\mathbf{X}_{m0}$ and $\mathbf{X}_{m1}$ and to understand the underlying cause behind this, we analyse the FAC for the robot base without the manipulator when evolved (artifically placed) along the trajectory of $\mathbf{X}_{m0}$ and $\mathbf{X}_{m1}$. The FAC plots are shown in figure 14(a) and 14(b). Similar to previous section, the normalised version of FAC is presented. It can be seen that while robot without the manipulator has higher FAC at some places, mobile manipulator on an average shows better performance. In fact, FAC for the robot base goes to zero at some places along $\mathbf{X}_{m0}$and $\mathbf{X}_{m1}$. For example consider figure14(a), where around 58th simulation step ($x = 2.24$,$y = 3.6$) the FAC for the vehicle goes to zero for the first time. Hence at this point, the path $\mathbf{X}_v$ and $\mathbf{X}_{m0}$ which were very similar prior to this point, bifurcates. The role of the manipulator in increasing the FAC at this particular point for the combined robot and manipulator system can be inferred from table 3. As can be seen from the table that the robot without the manipulator violates the permanent contact and no-slip stability constraints (33) while utilizing the reaction forces of the manipulator, the combined system of robot and manipulator is able to improve upon the constraint values. This further reiterates the fact that planning an appropriate motion for the manipulator is necessary for planning stable trajectories for the combined robot and manipulator system. This can also be inferred from figure 14(c) which shows the FAC plots along $\mathbf{X}_{m0}$ when the manipulator is kept fixed. The plot shows the FAC for various possible fixed positions and it

can be seen that no fixed position maintains a non-zero FAC along the entire trajectory.

Table 3: Comparison of only Robot base and Mobile Manipulator

	$\min N_i$	$\max(\lvert T_i \rvert - \rho N_i)$
$OnlyRobotbase$	-0.79	22.15
$MobileManipulator$	14.39	-10.67

6.3.2. Analysis of Motions of Combined Robot and Manipulator System

Figure 15(a) shows the 3D evolution of the mobile manipulator along $\mathbf{X}_{m0}$ where it moves from right to left towards the goal. Common intuition dictates that when the robot's base is moving up the slope, the most appropriate position for the manipulator is towards the front and vice-versa while coming down the slope. The manipulator tries to follow this as closely as possible provided it finds a feasible acceleration. For example consider the initial part of the manipulator's trajectory shown in a magnified view in figure 15(b) . It can be seen from the figure that the robot's base is moving up the slope in the encircled part C_1 but due to the lack of appropriate feasible acceleration, there is very little movement of the elbow joint(ϕ_1) (shown in yellow) and the shoulder joint (ϕ_2)(shown in pink). This can be confirmed by the plot of joint angles shown in figure 15(c) (sim step 0-20). However during the encircled part C_2, when the robot's base is moving down the slope, the elbow joint is able to rotate backwards and shoulder joint downwards(sim step 20-50). Moreover the manipulator moves in a way so as to compensate for the centripetal forces acting on the robot's base.

6.4. Comparison between FAC and Tip Over Stability Metric for Mobile Manipulator

In this section we compare FAC and Tip-Over as stability metric with regard to trajectory planning for articulated systems like a mobile manipulator. We validate that the ability of FAC to capture both stability and maneuverability is applicable for articulated systems as well. To this end, two sets of manipulator

trajectories were computed along $\mathbf{X}_{m0}$ and $\mathbf{X}_{m1}$. Similar to section 6.2 one set is based on the permanent contact and no-slip constraints (33) and maximizes FAC while the other set uses the Tip-Over constraints [4] and maximises tip-over margin.

Figure 16(a) gives the FAC and tip-over margin plot along the trajectories $\mathbf{X}_{m0}$ and $\mathbf{X}_{m1}$ for the set of manipulator motions aimed at maximizing FAC. It can be seen from the figure that maximizing FAC ensures that both tip-over margin and FAC remain above zero. However the situation is quite different in figure 16(b) which shows the results for the set of manipulator motions aimed at maximizing tip-over margin. It can be seen that while the tip-over margin has improved as compared to figure 16(a), FAC has drastically deteriorated. This further shows that FAC is a more conservative metric and its satisfaction generally ensures stability beyond what is predicted by tip over margin.

7. Conclusions and Future Work

In this paper we presented a novel metric called *Feasible Acceleration Count* or *FAC*. The metric was derived from the full 3D dynamics of a generic four wheeled robot on uneven terrain and gives a measure of the space of feasible accelerations at a given state of the robot. It was shown that *FAC* can act as an unified measure for robot maneuverability and stability. Moreover it was explained in detail, how *FAC* represents the space of control inputs available for the expansion of the tree in incremental sampling based trajectory planners like RRT. Thus *FAC* also quantifies the quality of state space exploration and consequently efficiency of motion planning on uneven terrains. We built on top of this aspect of *FAC* and proposed an incremental trajectory planner with RRT like data structure. The proposed planner was applied for motion planning of a generic four wheeled robot as well as articulated systems like mobile manipulators on uneven terrain.

The proposed trajectory planner however is computationally intensive because of two primary reasons. Firstly, the trajectory is only constructed incre-

mentally and hence it's convergence to the goal would be dictated by a great extent by the time step of integration of the evolution model at each iteration. Secondly, at each iteration the solution space of the differential constraints needs to be computed. In the current chapter a brute force search in the discretized control input space was employed to compute the solution space. Thus, one of our current primary focus is on developing efficient methodologies for computing the solution space of feasible accelerations. To this end, we are adapting the *non-linear time scaling* based methodology presented in our previous work [21], which computes a one shot solution space of feasible velocities and accelerations along a given path and combining it with the concept of *FAC*. The crux of the idea is that computing *FAC* along a path would reduce to computing the maximum and minimum feasible accelerations and can be reduced to solving a set of single variable inequalities through our *non-linear time scaling* methodology of [21].

[1] Lavalle, Steven M. "Rapidly-Exploring Random Trees: A New Tool for Path Planning." (1998).

[2] Kuffner, James J., and Steven M. LaValle. "RRT-connect: An efficient approach to single-query path planning." Robotics and Automation, 2000. Proceedings. ICRA'00. IEEE International Conference on. Vol. 2. IEEE, 2000.

[3] Kim, J., Ostrowski, J. P. (2003, September). Motion planning a aerial robot using rapidly-exploring random trees with dynamic constraints. In Robotics and Automation, 2003. Proceedings. ICRA'03. IEEE International Conference on (Vol. 2, pp. 2200-2205). IEEE.

[4] Papadopoulos, E., and Rey, D. A. (2000). The force-angle measure of tipover stability margin for mobile manipulators. Vehicle System Dynamics, 33(1), 29-48.

[5] Rey, D. A., and Papadoupoulos, E. G. (1997, September). Online automatic tipover prevention for mobile manipulators. In Intelligent Robots and Sys-

tems, 1997. IROS'97., Proceedings of the 1997 IEEE/RSJ International Conference on (Vol. 3, pp. 1273-1278). IEEE.

[6] Kubota, T., Kuroda, Y., Kunii, Y., Yoshimitsu, T. Path planning for a newly developed microver. In Robotics and Automation (ICRA), 2001 IEEE International Conference on (pp. 3710-3715). IEEE.

[7] Bonnafous, D., Lacroix, S., and Simon, T. (2001). Motion generation for a rover on rough terrains. In Intelligent Robots and Systems, 2001. Proceedings. 2001 IEEE/RSJ International Conference on (Vol. 2, pp. 784-789). IEEE.

[8] Mir, J. V., Dumonteil, G., Beck, C., and Dissanayake, G. (2010, October). A kyno-dynamic metric to plan stable paths over uneven terrain. In Intelligent Robots and Systems (IROS), 2010 IEEE/RSJ International Conference on (pp. 294-299). IEEE.

[9] Norouzi, M., Miro, J. V., and Dissanayake, G. (2012, October). Planning high-visibility stable paths for reconfigurable robots on uneven terrain. In Intelligent Robots and Systems (IROS), 2012 IEEE/RSJ International Conference on (pp. 2844-2849). IEEE.

[10] Cherif, M. (1999). Motion planning for all-terrain vehicles: a physical modeling approach for coping with dynamic and contact interaction constraints. Robotics and Automation, IEEE Transactions on, 15(2), 202-218.

[11] Shiller, Z., and Gwo, Y. R. (1991). Dynamic motion planning of autonomous vehicles. Robotics and Automation, IEEE Transactions on, 7(2), 241-249.

[12] Mann, M., and Shiller, Z. (2008, May). Dynamic stability of off-road vehicles: Quasi-3D analysis. In Robotics and Automation, 2008. ICRA 2008. IEEE International Conference on (pp. 2301-2306). IEEE.

[13] Kozlov, A., Gancet, J., Letier, P., Schillaci, G., Hafner, V. V., Fonooni, B., ... and Hellstrom, T. (2013, October). Development of a search and rescue

field robotic assistant. In Safety, Security, and Rescue Robotics (SSRR), 2013 IEEE International Symposium on (pp. 1-5). IEEE.

[14] Singh, A. K., Ghose, D., and Krishna, K. M. (2012, June). Optimum steering input determination and path-tracking of all-wheel steer vehicles on uneven terrains based on constrained optimization. In American Control Conference (ACC), 2012 (pp. 3611-3616). IEEE.

[15] English, A., Ross, P., Ball, D., and Corke, P. (2014, May). Vision based guidance for robot navigation in agriculture. In Robotics and Automation (ICRA), 2014 IEEE International Conference on (pp. 1693-1698). IEEE.

[16] Chakraborty, N., and Ghosal, A. (2005). Dynamic modeling and simulation of a wheeled mobile robot for traversing uneven terrain without slip. Journal of Mechanical Design, 127(5), 901-909

[17] Auchter, J., and Moore, C. A. (2008, May). Off-road robot modeling with dextrous manipulation kinematics. In Robotics and Automation, 2008. ICRA 2008. IEEE International Conference on (pp. 2313-2318). IEEE.

[18] Gattupalli, A., Eathakota, V. P., Singh, A. K., and Madhava Krishna, K. (2013). A simulation framework for evolution on uneven terrains for synchronous drive robot. Advanced Robotics, 27(8), 641-654.

[19] Singh, A. K., Krishna, K. M., and Eathakota, V. (2011, December). Planning stable trajectory on uneven terrain based on Feasible Acceleration Count. In Decision and Control and European Control Conference (CDC-ECC), 2011 50th IEEE Conference on (pp. 6373-6379). IEEE.

[20] Singh, A. K., and Krishna, K. M. (2013, November). Coordinating mobile manipulator's motion to produce stable trajectories on uneven terrain based on feasible acceleration count. In Intelligent Robots and Systems (IROS), 2013 IEEE/RSJ International Conference on (pp. 5009-5014). IEEE.

[21] Singh, A. K., Krishna, K. M., and Saripalli, S. (2012, October). Planning trajectories on uneven terrain using optimization and non-linear time scal-

ing techniques. In Intelligent Robots and Systems (IROS), 2012 IEEE/RSJ International Conference on (pp. 3538-3545). IEEE.

[22] Bajaj, C. L., Bernardini, F., ands Xu, G. (1995, September). Automatic reconstruction of surfaces and scalar fields from 3D scans. In Proceedings of the 22nd annual conference on Computer graphics and interactive techniques (pp. 109-118). ACM.

[23] Amenta, N., Bern, M., and Kamvysselis, M. (1998, July). A new Voronoi-based surface reconstruction algorithm. In Proceedings of the 25th annual conference on Computer graphics and interactive techniques (pp. 415-421). ACM.

[24] Prokos, A., G. Karras, and E. Petsa. "Automatic 3D surface reconstruction by combining stereovision with the slit-scanner approach." hand 2 (2010): 2.

[25] Craig, J. J. (1989). Introduction to robotics (Vol. 7). Reading, MA: Addison-Wesley.

[26] Chan, C. C. (2007). The state of the art of electric, hybrid, and fuel cell vehicles. Proceedings of the IEEE, 95(4), 704-718. Chicago

[27] Jones, J., Karampetakis, N. P., and Pugh, A. C. (1998). The computation and application of the generalized inverse via Maple. Journal of Symbolic Computation, 25(1), 99-124.

[28] http://robonaut.jsc.nasa.gov/

[29] Huang, Q. Sugano, S. Kazuo, T,." Motion planning for Mobile Manipulators considering Stability and Task constraints" in Proc of ICRA 1998 pp 2192-2198

[30] Huang, Q. Kazuo, T Sugano, S " Coordinated Motion planning for a Mobile Manipulator considering Stability and Manipulation" in *International Journal of Robotics Research* August 2000 vol 19 No 8 pp 732-742

[31] Alipour, K., Moosavian, S. A. A., and Bahramzadeh, Y. (2008, July). Postural stability evaluation of spatial wheeled mobile robots with flexible suspension over rough terrains. In Advanced Intelligent Mechatronics, 2008. AIM 2008. IEEE/ASME International Conference on (pp. 241-246). IEEE.

[32] Alipour, K., and Moosavian, S. A. A. (2012). Effect of Terrain Traction, Suspension Stiffness and Grasp Posture on the Tip-Over Stability of Wheeled Robots with Multiple Arms. Advanced Robotics, 26(8-9), 817-842.

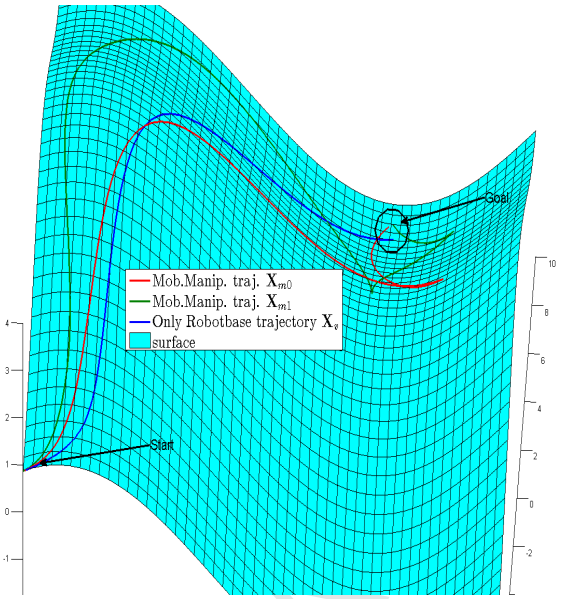

(a)

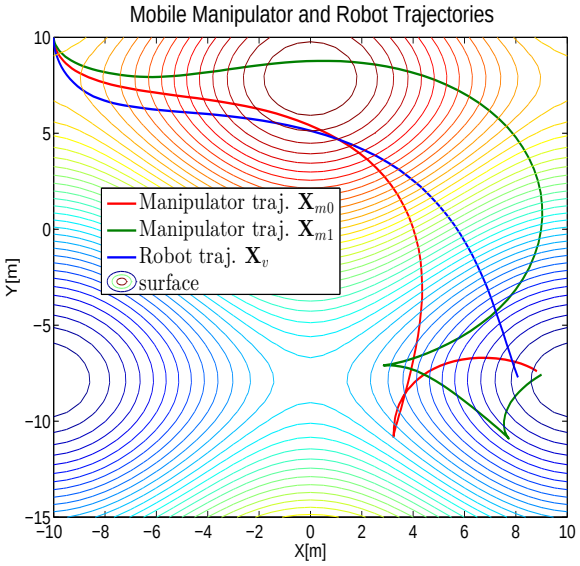

(b)

Figure 13: (a),(b): FAC based trajectories obtained for only the robot base and the combined robot base plus manipulator system

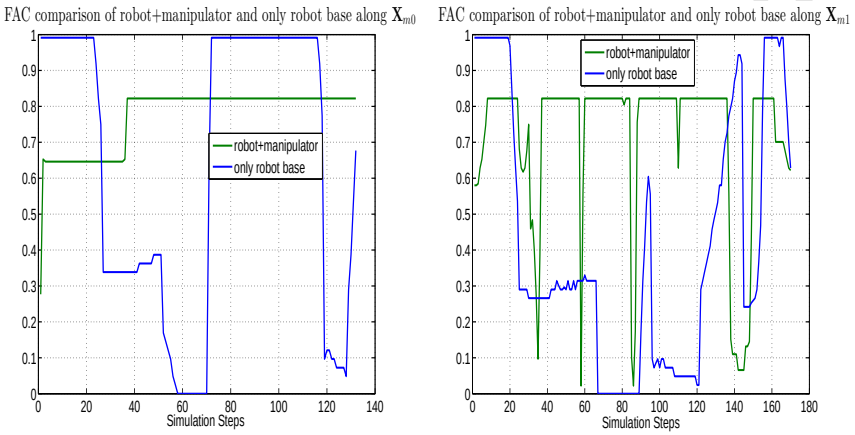

(a) (b)

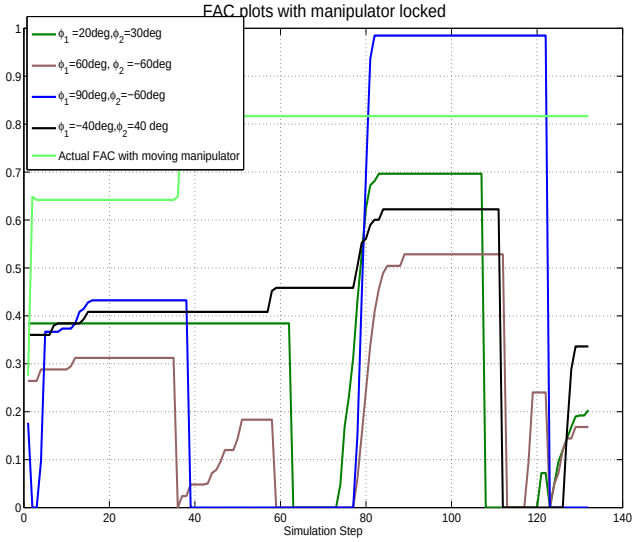

(c)

Figure 14: (a), (b): *FAC* variation of only robot base along the mobile manipulator trajectories. The figures clearly show the role of manipulator's motion in improving *FAC*, as mobile manipulator is stable at various points along the trajectories where only robot base would loose stability. (c): *FAC* variation along the obtained mobile manipulator trajectories if the manipulator is kept locked at various different configuration. It can be seen that no manipulator configuration can ensure a non-zero *FAC* along the entire trajectory, thus further re-iterating the need of proper coordination between the manipulator and robot base motion.

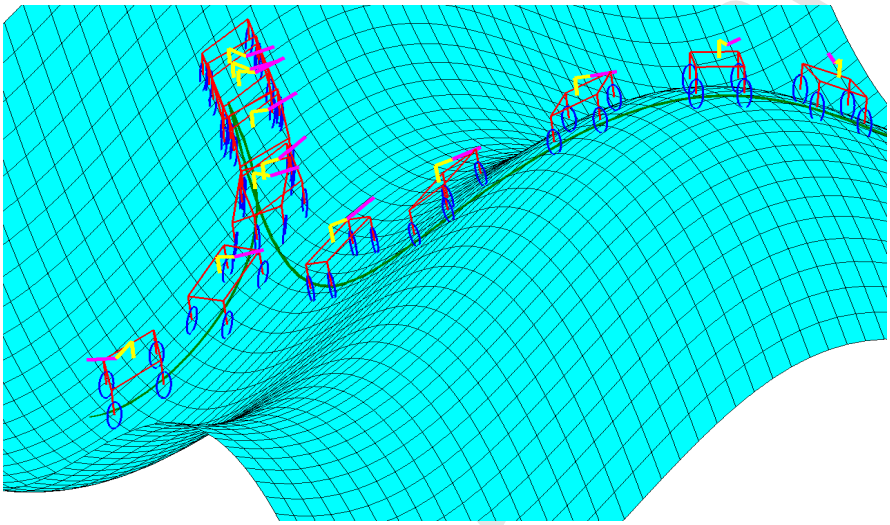

(a)

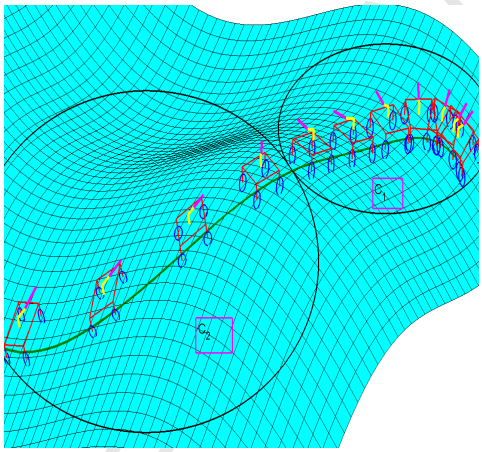

(b)

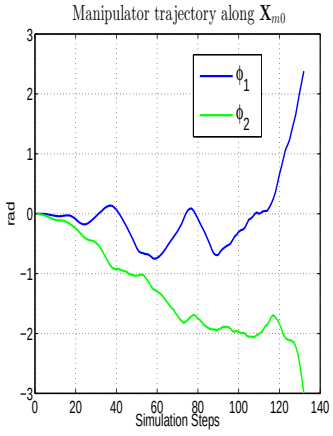

(c)

Figure 15: (a),(b): Evolution of mobile manipulator on uneven terrain. (c): Plot of manipulator configuration

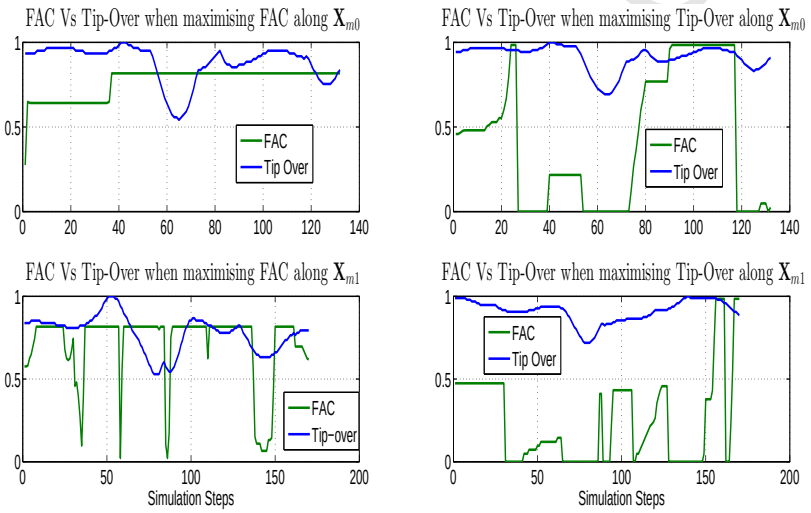

(a) (b)

Figure 16: (a),(b): Figures showing that the conservativeness of *FAC* over *tip-over* stability concept is valid for even articulated robotic systems like mobile manipulator. Along each trajectories obtained for the mobile manipulator, two sets of manipulator trajectories were computed. One set optimizes *FAC* while other set optimizes *tip-over* margin. It can be seen that optimizing *FAC* also ensures that *tip-over* remains above zero. However *FAC* goes to zero at various points along the trajectory if the manipulator motion is aimed at maximising *tip-over*

***Biography of each author**

K. Madhava Krishna is an Associate Professor and head of the Robotics Research Centre at IIIT-Hyderabad, India. He obtained his Bachelors in Electrical and Electronics Engineering and Masters in Electronics Engineering from Birla Institute of Technology, Pilani, India in 1996 and 1998 respectively. He obtained his PhD from IIT-Kanpur in 2001. From 2001-2002 he was a post-doctoral researcher at LAAS-CNRS. Toulouse, France. His research interests include mobile robot motion planning, SLAM, and outdoor navigation of mobile robots.

***Biography of each author**

Arun Kumar Singh is a PhD candidate in Robotics Research Centre, IIIT-Hyderabad, India. His research interests include motion planning with differential constraints with application to uneven terrain navigation and multi-robot trajectory generation. From 2009-2010 he was associated with Aerospace Engineering Department , IISc –Bangalore, India. He received his Bachelors in Mechanical Engineering from NIT Durgapur, India in 2009.

*Photo of each author

***Photo of each author**

- A novel dynamic stability metric called Feasible Acceleration Count(FAC) is proposed
- FAC gives a measure of the space of feasible/stable accelerations at a given state.
- It acts as a unified metric for quantifying stability and maneuverability of robot.
- It quantifies the efficiency of state space exploration in sampling based planners.
- An incremental planner with a novel node selection criteria based on FAC is proposed